Proceedings of the 7th International Symposium on Cavitation
CAV2009
August 17-22, 2009, Ann Arbor, Michigan, USA

CAV2009 – Paper No. 15

Prediction of Impeller Speed Dependence of Cavitation Intensity in Centrifugal Pump Using Cavitating Flow Simulation with Bubble Flow Model

Masashi Fukaya
Hitachi, Ltd.
Mechanical Engineering Research Laboratory
832-2, Horiguchi, Hitachinaka, Ibaraki, 312-0034, Japan
Tel. +81-29-353-3489
Fax. +81-29-353-3865
E-mail: masashi.fukaya.kp@hitachi.com

Yoshiaki Tamura
Toyo University
Department of Computational Science and Engineering
2100, Kujirai, Kawagoe, Saitama, 350-8585, Japan
Tel. +81-492-39-1465
Fax. +81-492-31-5026
E-mail: tamtam@eng.toyo.ac.jp

Yoichiro Matsumoto
University of Tokyo
Department of Mechanical Engineering
7-3-1, Hongo, Bunkyo-ku, Tokyo, 113-8656, Japan
Tel. +81-3-5841-6286
Fax. +81-3818-0835
E-mail: ymats@fel.t.u-tokyo.ac.jp

ABSTRACT

We developed a numerical method of estimating not only cavitation erosion area but also cavitation intensity that depends on the impeller speed of pumps. Our numerical simulation code with a 'bubble flow model' simulates the bubble pressure and the bubble nuclei distribution in a cavitating flow in detail. We simulated impulsive bubble pressure that varied within microseconds in a centrifugal pump. The cavitation intensity was estimated by analyzing the bubble pressure and the bubble nuclei distribution.

The erosion area on the impeller blade in our pump test was visualized by using a method involving dye. The plastic deformation rate of an aluminum sheet attached in the erosion area was measured, and the cavitation intensity was estimated using an experimental database. The erosion area and cavitation intensity were measured at high and low impeller speeds. The erosion areas were both located on the suction side of the impeller blade, and they were distributed between the shroud and the mid-point of the blade near the leading edge. The measured cavitation intensity at high-speed was twice that at low-speed.

The predicted areas of high cavitation intensity agreed well with the erosion areas in the experiment though the predicted areas slightly shifted to the leading edge. The predicted cavitation intensity at high-speed doubled that at low-speed as well as the experimental result. Therefore, we confirmed that the numerical method of estimating cavitation intensity was accurate.

Next, we added three calculations while changing the impeller speed to obtain a function of cavitation intensity variations. The predicted function was a function of the impeller speed to the power, and this also corresponded to the experimental. Our code is thus effective for estimating the cavitation intensity that increases on the suction side of the impeller blade in a centrifugal pump when the impeller speed is changed.

INTRODUCTION

Downsized pumps are needed to increase impeller speed to satisfy required specifications of the total head and flow rate. As the increase in impeller speed raises the risk of cavitation erosion, it is important to predict the cavitation erosion to maintain the reliability of pumps. Cavitation intensity is defined as the impact power per unit area when the cavitation bubbles collapse. The cavitation intensity should be experimentally or numerically estimated since it has a strong correlation with the cavitation erosion.

We developed an experimental method of predicting the maximum erosion rate in actual pumps [1]. This was based on a method involving the use of an aluminum sheet [2], and the following two contents were improved. The one was that a new scaling law on cavitation intensity between model and actual pumps was introduced. The other was that the relation between the cavitation intensity and the histogram on bubble impact force and frequency was also applied taking the threshold of impact force into consideration [3]. By using the developed method, the cavitation intensity can be estimated from the measured rate of plastic deformation of an aluminum sheet attached to an impeller blade.

A 'bubble flow model' is one of the most representative models of cavitation for numerical simulations. A remarkable feature is that abrupt time-variations in the radius and inner pressure of bubbles can be simulated by using the Rayleigh-Plesset equation in a cavitating flow. The cavitation intensity can be estimated based on the bubble radius or the bubble pressure. Zima et al. evaluated the cavitation intensity by calculating an impact force of cavitation. The impact force was obtained based on the rate of variations in the bubble radius. In their method, the distribution of bubble number density was not considered. They predicted the erosion area on the impeller blade of a mixed-flow pump [4]. We defined numerical cavitation intensity based on the time-variation in the bubble pressure considering the bubble number density, and predicted the erosion area on the impeller blade of a centrifugal pump [5]. However, variations in the cavitation intensity under different operating conditions have not yet been investigated.

We attempted to predict not only the erosion area but also the variations in the cavitation intensity under different operating conditions by using the numerical simulation with the bubble flow model. The static pressure at the suction pipe was not reflected to the inlet boundary conditions for the bubble radius and the bubble pressure in the previous study [5]. The inlet boundary conditions were improved with the static pressure at the suction pipe to estimate accurately the cavitation intensity in the present study. The cavitation intensity depending on the impeller speed of a centrifugal pump was estimated, and was verified with that measured by using the aluminum sheet method [1]. We further investigated the power law of the cavitation intensity in terms of the impeller speed. The function we obtained from the simulation was compared with reference data from the Turbomachinery Society of Japan [6].

NUMERICAL METHOD

Bubble Flow Model and Cavitation Intensity

The following assumptions concerning the bubbles in a flow were made in the simulation code.

The liquid phase is uncompressible and the gas phase consisting of spherical bubbles is compressible. No coalescence or breakup of bubbles occurs. The bubbles are filled with vapor and non-condensable gas. The pressure of the non-condensable gas varies in the isothermal expansion and the adiabatic contraction processes that represent evaporation and condensation on the bubble surface [7]. The density and momentum of the gas phase are sufficiently small to be negligible.

The governing equations are described in a generalized coordinate system as: the momentum equation of bubble flow,

$$\frac{\partial(\rho_L f_L u_{Li})}{\partial t} + J\frac{\partial(\rho_L f_L u_{Li} U_{Li}/J)}{\partial \xi_j} = -\nabla_i p + \nabla_j(\mu\nabla_j u_{Li}) + \frac{1}{3}(\mu\nabla_k u_{Lk}) - \rho_L\{2\varepsilon_{ijk}\Omega_j u_{Lk} + \varepsilon_{ijk}\Omega_j(\varepsilon_{klm}\Omega_l r_m)\}\ , \qquad (1)$$

where the liquid and gas velocities mean the relative velocities in a rotating coordinate system; the transport equation for the bubble number density is,

$$\frac{\partial n_G}{\partial t} + J\frac{\partial(n_G U_{Gi}/J)}{\partial \xi_j} = 0 \quad , \qquad (2)$$

where the bubble number density, n_G, is the number of bubbles in a unit volume, and a pressure equation is based on pseudo-compressibility, which is derived from the conservation of the volumetric fractions of the liquid and gas phases,

$$\frac{1}{c^2}\frac{\partial p}{\partial t} + \nabla_j f_L u_{Lj} + \nabla_j f_G u_{Gj} - 4\pi {r_G}^2 n_G \frac{Dr_G}{Dt} = 0 \quad . \qquad (3)$$

The volumetric motion of a bubble is described by the Rayleigh-Plesset equation [8],

$$r_G\frac{D^2 r_G}{Dt^2} + \frac{3}{2}\left(\frac{Dr_G}{Dt}\right)^2 = \frac{p_B - p_L}{\rho_L} + \frac{1}{4}(u_{Li} - u_{Gi})(u_{Li} - u_{Gi})\ , \qquad (4)$$

$$p_B = p_G + p_v - \frac{2T}{r_G} - 4\mu\frac{1}{r_G}\frac{Dr_G}{Dt} \quad , \qquad (5)$$

$$p_G {r_G}^3 = const. \quad \left(\frac{Dr_G}{Dt} > 0\right) \quad , \qquad (6)$$

$$p_G {r_G}^{3\kappa} = const. \quad \left(\frac{Dr_G}{Dt} < 0\right) \quad , \qquad (7)$$

where both T (= 0.072 N/m) and p_v (= 2300 Pa) are constant. The viscosity, μ, is assumed to be the same as that of water ($\mu = 1.0\times10^{-3}$ Pa s). The specific heat ratio, κ, is 1.4. The non-condensable gas pressure, p_G, varies in the isothermal expansion and adiabatic contraction processes (Eqs. (6) and (7)) [7].

The occurrence of cavitation is expressed as an increase in the void fraction, which is calculated by,

$$f_G = \frac{4}{3}\pi {r_G}^3 n_G \quad . \qquad (8)$$

The void fraction is the product of the volume of a bubble by the bubble number density.

The translational motion of a bubble is solved taking into consideration the force balance of the bubble,

$$F_{Ai} + F_{pi} + F_{Di} + F_{Li} + F_{Coi} + F_{Cei} = 0\ , \qquad (9)$$

where F_{Ai} is the added mass force,

$$F_{Ai} = \frac{4}{3}\pi\beta\left\{\left(\frac{\partial(\rho_L {r_G}^3 u_{Gi})}{\partial t} + U_{Gj}\frac{\partial(\rho_L {r_G}^3 u_{Gi})}{\partial \xi_j}\right)\right\} - \left\{\left(\frac{\partial(\rho_L {r_G}^3 u_{Li})}{\partial t} + U_{Lj}\frac{\partial(\rho_L {r_G}^3 u_{Li})}{\partial \xi_j}\right)\right\} \quad , \qquad (10)$$

β is a constant of 0.5 for a spherical bubble, and F_{pi} is the force of acceleration of the surrounding fluid,

$$F_{Pi} = -\frac{4}{3}\pi\ \rho_L r_G^{\ 3}\left(\frac{\partial u_{Li}}{\partial t} + U_{Lj}\frac{\partial u_{Li}}{\partial \xi_j}\right) \quad . \qquad (11)$$

F_{Di} and F_{Li} are the drag and lift forces [9][10],

$$F_{Di} = \frac{1}{2}\pi\ \rho_L\, r_G^{\ 2} C_D\, |u_G - u_L|\,(u_{Gi} - u_{Li}) \quad , \qquad (12)$$

$$F_{Li} = \frac{1}{2}\pi\ \rho_L r_G^{\ 2}\ C_L |u_G - u_L|\,\varepsilon_{ijk}\,\omega_{Lk}(u_{Gj} - u_{Lj})/|\omega_L| \quad , \qquad (13)$$

$$C_D = \frac{24}{\mathrm{Re}_{bub}}(1 + 0.15\,\mathrm{Re}_{bub}^{\ 0.687}) \quad , \qquad (14)$$

$$\mathrm{Re}_{bub} = \frac{2 r_G\,\rho_L\,|u_G - u_L|}{\mu_L} \quad , \qquad (15)$$

$$C_L = 0.59\left(\frac{|\omega_L|\, r_G}{|u_G - u_L|}\right)^{0.25} \quad , \qquad (16)$$

where ω_L is the vorticity vector. F_{Coi} and F_{Cei} are the Coriolis' force and centrifugal force,

$$F_{Coi} = \frac{8}{3}\pi\ \rho_L r_G^{\ 3}\left\{\beta\varepsilon_{ijk}\Omega_j u_{Gk} - (1+\beta)\varepsilon_{ijk}\Omega_j u_{Lk}\right\} \quad , \qquad (17)$$

$$F_{Cei} = -\frac{4}{3}\pi\ \rho_L r_G^{\ 3}\left\{\varepsilon_{ijk}\Omega_j\left(\varepsilon_{klm}\Omega_l r_m\right)\right\} \quad . \qquad (18)$$

The velocity of a bubble relative to the liquid phase is solved using Eqs. (9)-(18). Further details on the governing equations and the algorithm for calculation are described by Tamura et al. [11].

The Reynolds number for the flow in a centrifugal pump in the present study was over 4.6×10^5, where the Reynolds number was based on the diameter of the suction pipe and the average liquid velocity in the suction pipe. However, no turbulent models were used in the simulation code to reduce the calculation time.

The cavitation intensity, I, is numerically defined as

$$I = \sum_{p_B \geq p_{Bth}} \frac{p_B^{\ 2} n_G \Delta V \Delta t}{2\rho_L C} \Big/ \Delta T \quad , \qquad (19)$$

where p_{Bth} is the threshold bubble pressure [5]. Equation (19) is similar to the generally defined cavitation intensity as follows,

$$I = \frac{p_c^{\ 2}}{2\rho_L C} \quad , \qquad (20)$$

where p_c is the bubble collapse pressure [3]. In the present simulation, the bubble collapse pressure was not calculated, but was represented by the bubble pressure. The bubble number density represents a bubble cluster. The threshold bubble pressure is analogous to the threshold of the impact force affecting the cavitation erosion [3]. We temporarily fixed the threshold at 0.3 MPa. When the bubble pressure exceeded the threshold, the cavitation intensity was estimated using Eq. (19) in the mesh nearest to the blade surface.

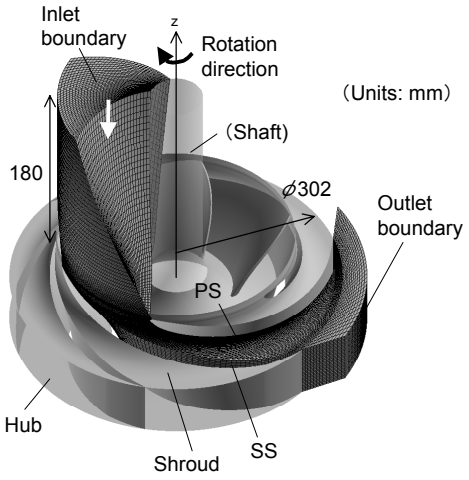

Fig. 1 Simulated region and boundary conditions

Pump Specifications and Calculation Conditions

We again applied our simulation code to the centrifugal pump that was investigated in the previous study [5]. The impeller had six blades that had a shroud. The maximum diameter of the impeller was 302 mm, and the hub diameter was 78 mm. The pump had a volute casing downstream of the impeller. The flow rate at the best efficiency point was 7.6 m^3/min.

Figure 1 shows the numerical mesh and boundary conditions. The region between the pressure and suction sides of the impeller blades was investigated using periodic boundaries. A suction pipe of 180 mm was connected to the impeller section. A fan-shaped downstream channel of 50 mm in the radial direction was connected to the impeller section instead of the volute casing. There were a total of 184,000 grids.

The liquid and gas velocities, the bubble number density, the bubble radius and the bubble pressure were uniformly distributed on the inlet boundary. The inlet velocities of the liquid and gas phases were 2.12 m/s at the standard impeller speed, N_0. The bubble number density was 2.39×10^{11} m^{-3}. (The initial bubble number density in all simulated region was also 2.39×10^{11} m^{-3}.) The procedure for setting the values of the bubble radius and the bubble pressure will be explained in the next section in detail. The static pressure was uniform on the outlet boundary, and varied to adjust the *NPSH* conditions.

The rate of the impeller speed, N, against the standard impeller speed, N_0, is called 'impeller speed rate,' N/N_0, in the present paper. The simulation was conducted under conditions of N/N_0 = 1.00, 1.17, 1.33, 1.50, and 1.67. The inlet velocity and *NPSH* were varied corresponding to the impeller speed in accordance with the pump similarity laws.

Bubble Radius and Pressure at Inlet Boundary

The bubble radius in the previous study [5] was fixed at 1.0×10^{-5} m on the inlet boundary. The non-condensable gas pressure, p_G, was assumed to be 1.0×10^5 Pa on the inlet boundary, and the bubble pressure, p_B, was given by Eq. (5). However, the bubble radius and the bubble pressure on the inlet boundary should be adjusted in response to the suction pressure depending on pump operating conditions. The bubble radius

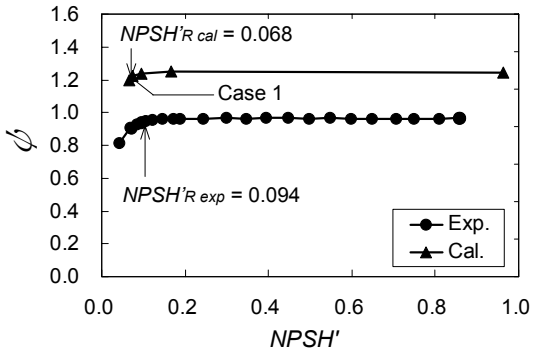

Fig. 2 Cavitation performance of centrifugal pump (N/N_0= 1.00, and $Q/Q_{\eta max}$= 0.60)

and the bubble pressure on the inlet boundary in the present study were determined using the following procedure.

Assuming the quasi-equilibrium concerning the liquid and gas phases, $p_B = p_L$ is instantly achieved. Then, the following equations are derived from Eq. (5),

$$p_{L\infty} = p_{G\infty} + p_v - \frac{2T}{r_{G\infty}} \quad , \qquad (19)$$

$$p_{L1} = p_{G1} + p_v - \frac{2T}{r_{G1}} \quad , \qquad (20)$$

where the subscript, ∞, means the point at infinity and the subscript 1 means the inlet boundary. The difference between $p_{L\infty}$ and p_{L1} is,

$$p_{L1} - p_{L\infty} = p_{G1} - p_{G\infty} - 2T\left(\frac{1}{r_{G1}} - \frac{1}{r_{G\infty}}\right) . \qquad (21)$$

Equations (6) and (7) are described as,

$$p_{G1} = p_{G\infty}\left(\frac{r_{G\infty}}{r_{G1}}\right)^{3\kappa} \quad (p_{L1} > p_{L\infty}) \quad , \qquad (22)$$

$$p_{G1} = p_{G\infty}\left(\frac{r_{G\infty}}{r_{G1}}\right)^{3} \quad (p_{L1} < p_{L\infty}) \quad . \qquad (23)$$

At the infinity point, $r_{G\infty} = 1.0\times10^{-5}$ m and $p_{G\infty} = 1.0\times10^5 - p_v + 2T/r_{G\infty}$ Pa (i.e., $p_{B\infty} = 1.0\times10^5$ Pa) are assumed; $p_{L\infty}$ is then obtained from Eq. (19). When p_{L1} is known based on the numerical results, p_{G1} and r_{G1} are obtained by calculating Eqs. (21) and (22), or Eqs. (21) and (23), simultaneously. Finally, p_B (= p_L) is calculated with Eq. (20).

Four stage calculations (a-d) were conducted in the present study:

(a) Under all pump operating conditions, the flow in the pump was formed assuming the quasi-equilibrium concerning the liquid and gas phases. The tentative conditions of r_{G1} = 1.0×10^{-5} m and $p_{G1} = 1.0\times10^5$ Pa were given on the inlet boundary. At this stage, bubble pressure variations were not calculated in detail.

(b) p_{L1} was extracted after stage (a). Then, p_{G1} and r_{G1} were obtained with the above procedure.

(c) Assuming the same quasi-equilibrium at stage (a), the flow in the pump was re-formed under p_{G1} and r_{G1} conditions obtained at stage (b).

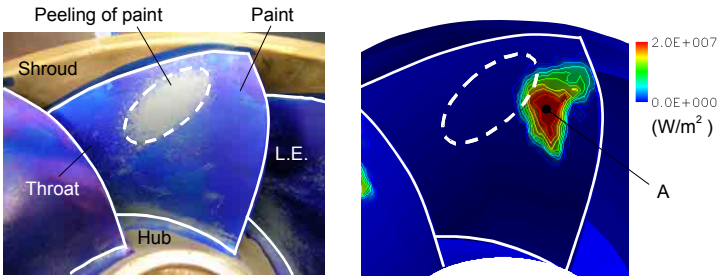

(a) Erosion area in experiment (b) Cavitation intensity distribution

Fig. 3 Comparison of experimental erosion area and predicted high-cavitation intensity area (N/N_0= 1.00)

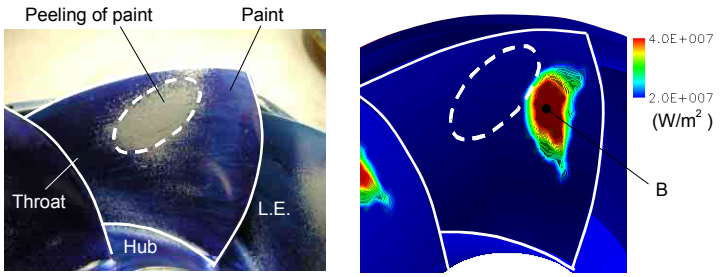

(a) Erosion area in experiment (b) Cavitation intensity distribution

Fig. 4 Comparison of experimental erosion area and predicted high-cavitation intensity area (N/N_0= 1.17)

(d) Then, no quasi-equilibrium was assumed to calculate the bubble pressure variations in detail.

RESULTS AND DISCUSSION

Cavitation Performance

Figure 2 shows the cavitation performance of the centrifugal pump under conditions of N/N_0 = 1.00 and $Q/Q_{\eta max}$ = 0.6. The *NPSH* and total head were divided by $U_t^2/(2g)$ to make them dimensionless, i.e., *NPSH*' and ψ. In the experiment, the total head decreased when the *NPSH*' was below $NPSH_{Rexp}$' (= 0.094), while it remained nearly constant when the *NPSH*' was over $NPSH_{Rexp}$'. The predicted $NPSH_{Rcal}$' was 0.068, and the predicted total head variations qualitatively agreed with those from the experiment. The sheet cavitation was not precisely simulated in the present study because the cavity surface was not modelized. Therefore, the volume of the cavitating region was underestimated as $NPSH_{Rcal}$' < $NPSH_{Rexp}$'.

The predicted total head exceeded the experimental one since the total head in the experiment included the effect of loss caused by flow in the volute casing. Although the predicted cavitation performance was not necessarily in good quantitative agreement with that from the experiment, the change in flow pattern caused by the occurrence of cavitation around the impeller blades was qualitatively simulated.

The discussion in the following sections is based on the numerical results in Case 1 (N/N_0 = 1.00) and other four cases under conditions of N/N_0 = 1.17, 1.33, 1.50, and 1.67. In the latter four cases, the inlet velocity and *NPSH* conditions were

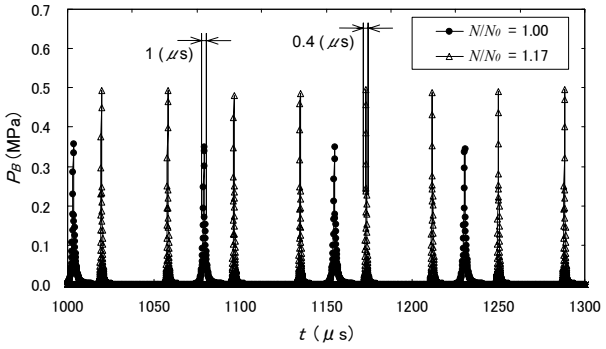

Fig. 5 Transient bubble pressure at points A and B in Figs. 3 (b) and 4(b)

Table 1 Peak characteristics of bubble pressure in Fig. 5

N/N_0	P_{Bmax} (MPa)	Δt_w (μs)	Δt_{p-p} (μs)
1.00	0.35	1	75
1.17	0.5	0.4	38

varied from those in Case 1 in accordance with the pump similarity laws.

Cavitation Erosion Area and Cavitation Intensity Distribution

Figures 3 and 4 show the cavitation erosion area and the cavitation intensity distribution at N/N_0 = 1.00 and 1.17. The erosion area on the impeller blade in the experiment was visualized by using a method involving dye. A blue dye was painted on the suction side of the impeller blade, and the pump was continuously operated for four hours at N/N_0 = 1.00 and for three hours at N/N_0 = 1.17. The erosion area was specified since the dye was locally peeled off under the influence of the impulsive high pressure generated when the cavitation bubbles collapsed. In both cases at N/N_0 = 1.00 and 1.17, the oval-shaped erosion areas were located at the center of the region between the throat and the leading edge of the blade, and were located between the shroud and the mid-point of the blade. The same distribution in the erosion area was caused by the similarity in flows. The shroud in Fig. 4 was temporarily removed when the photograph was taken.

High cavitation intensity regions appeared in the numerical results between the shroud and the mid-point of the blade. The high cavitation intensity regions shifted to the leading edge of the blade compared to the erosion areas. Although there was the positional shift in the high cavitation intensity region to the reading edge, these results indicate that the erosion areas were accurately predicted as well as in the previous study [5]. The variations in the cavitation intensity depending on the impeller speed were investigated and are discussed in the following sections.

Bubble Pressure, Bubble number density and Cavitation Intensity

Figure 5 shows the time-variations in the bubble pressure at points A and B in Figs. 3(b) and 4(b), where the cavitation intensity was maximum on the suction side of the blade. The

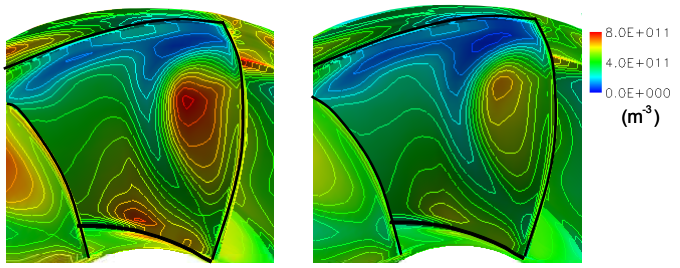

(a) N/N_0= 1.00 (b) N/N_0= 1.17

Fig. 6 Distribution of bubble number density

bubble pressure had periodical impulsive peaks. The maximum value of the peak, p_{Bmax}, the half width of the peak, Δt_w, and the time duration of the neighboring peaks, Δt_{p-p}, are summarized in Table 1. With increasing impeller speed, p_{Bmax} increased while Δt_w and Δt_{p-p}, decreased. This means that the bubbles expanded and contracted more abruptly and frequently when the impeller speed was increased.

Figure 6 shows the distributions in the bubble number density at N/N_0 = 1.00 and 1.17. The bubbles in both results were accumulated near the leading edge on the suction side of the blade, while the accumulation at N/N_0 = 1.17 was just reduced compared with that at N/N_0 = 1.00. The accumulated regions of the bubbles were distributed similarly with the high cavitation intensity regions in Figs. 3(b) and 4(b).

The cavitation intensities at points A and B in Figs 3(b) and 4(b) were estimated to reach 2.2×10^5 W/m^2 and 4.7×10^5 W/m^2. The cavitation intensity at N/N_0 = 1.17 was 2.1 times that at N/N_0 = 1.00 since the effect from the increase in the bubble pressure was larger than that of the decrease in the bubble accumulation as indicated in Figs. 5 and 6.

The cavitation intensities in the experiment were estimated based on the plastic deformation rate of the aluminum sheet attached within the peeling area of the blue dye [1]. The measured cavitation intensity at N/N_0 = 1.17 was 2.4 times that at N/N_0 = 1.00. Although the predicted value of 2.1 times was slightly smaller than the experimental value of 2.4 times, we verified that the variations in the cavitation intensity depending on the impeller speed were quantitatively estimated with our simulation code.

Dependence of Cavitation Intensity on Impeller Speed

In the previous study [1], the following empirical equation was obtained from Ref. [6]:

$$I / I_0 = \left(N / N_0\right)^{(c-2)b} \left(P_w / P_{w0}\right) \quad . \qquad (24)$$

where b and c are the empirical constants as will be explained later. P_w is the water power of the pump at the best efficiency point. The subscript, 0, means the standard condition. Based on the pump similarity laws,

$$P_w / P_{w0} = \left(N / N_0\right)^3 \quad , \qquad (25)$$

Eq. (24) is expressed as

$$I / I_0 = \left(N / N_0\right)^x \quad , \qquad (26)$$

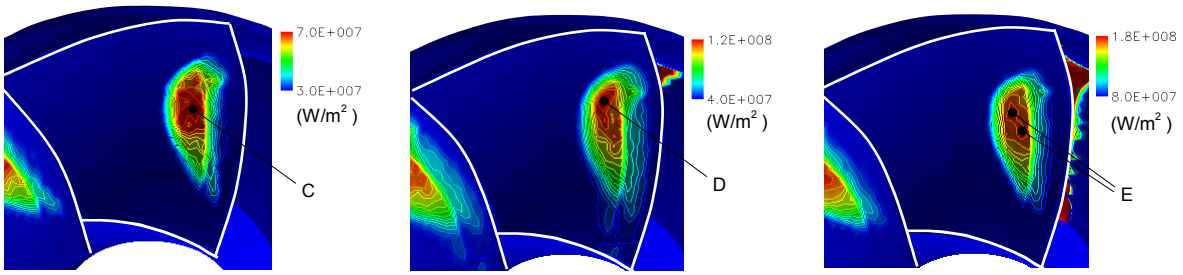

(a) N/N_0 = 1.33 (b) N/N_0 = 1.50 (c) N/N_0 = 1.67

Fig. 7 Cavitation intensity distribution at different impeller rotational speeds

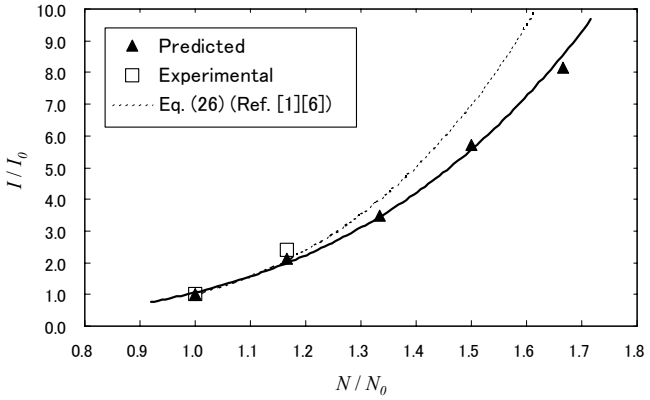

Fig. 8 Dependence of cavitation intensity on impeller rotational speed

$$x = (c-2)b+3 \quad . \qquad (27)$$

Equation (26) indicates that the cavitation intensity ratio, I / I_0, is N/N_0 to the power of the empirical constant, x.

Figure 7 shows the cavitation intensity distributions at N/N_0 = 1.33, 1.50, and 1.67. All the high cavitation intensity regions were distributed near the leading edge between the shroud and the mid-point of the blade as well as those at N/N_0 = 1.00 and 1.17.

Figure 8 shows the dependence of the cavitation intensity on the impeller speed. The predicted cavitation intensities were obtained at points A - E as shown in Figs. 3(b), 4(b), and 7, where the cavitation intensity was maximum under each N/N_0 condition. I_0 means the predicted or measured cavitation intensity at N/N_0 = 1.00. The solid line in Fig. 8 is the least-squares line based on the five numerical results,

$$I / I_0 = 1.06 \left(N / N_0\right)^{4.09} \quad . \qquad (28)$$

Equation (28) shows that I / I_0 is a function of N/N_0 to the power. This means that the numerical results were valid concerning the power law. Furthermore, the power-law index, x, was investigated as follows.

The TSJ Guideline [6] states that b = 1.58 was measured in a pump having a centrifugal impeller and a volute casing. The empirical constant, b, was obtained based on the measured cavitation intensities under different flow rate conditions. The constant, b, was not measured in the present pump. However, b = 1.58 was adopted here since the type of present pump was similar to that in the guideline [6], i.e., both pumps were centrifugal volute pumps.

The empirical constant, c, was the power-law index of the vibration acceleration measured on the volute casing by using a vibration acceleration sensor [6]. In the present pump, c = 3.14 was obtained by the vibration acceleration measurement. Therefore, $x = (c\text{-}2)b+3$ = 4.80 was obtained by using Eq. (27) based on b = 1.58 and c = 3.14. The dotted line in Fig. 8 indicates the values calculated with Eq. (26) at x = 4.80. The numerical results underestimated the cavitation intensity, and the difference between the predicted cavitation intensity and that calculated with Eq. (26) at x = 4.80 rose with increasing impeller speed. However, the predicted cavitation intensity agreed well with the data based on the guideline [6]. This means that the numerical results were valid concerning the power-law index.

CONCLUSION

Cavitation intensity variations depending on the pump impeller speed were predicted by using a cavitating flow simulation with the bubble flow model. The simulation was applied to a pump having a centrifugal impeller and a volute casing under improved conditions of the bubble radius and the bubble pressure on the inlet boundary.

(1) When the impeller speed rate, N/N_0, was increased from N/N_0 = 1.00 to N/N_0 = 1.17, the predicted cavitation intensity at high-speed was 2.1 times that at low-speed, while the measured cavitation intensity varied to become 2.4 times.

(2) The predicted cavitation intensity ratio at N/N_0 = 1.00, 1.17, 1.33, 1.50, and 1.67 was described as a function of N/N_0 to the power, which corresponded to the empirical function. The predicted power-law index of 4.09 agreed well with that from the experiment of 4.80.

There results confirmed our simulation and method of estimating the cavitation intensity were valid.

NOMENCLATURE

c	Coefficient for pseudocompressibility
C	Sound velocity in water (m/s)
f	Volume fraction (-)
$\hat{E}, \hat{F}, \hat{G}$	Fluxes in ξ, η, and ζ directions
F	Force (N)

g	Acceleration due to gravity (m/s^2)
H	Head (m)
$\hat{H}$	Source term
I	Cavitation intensity (W/m^2)
n	Bubble number density (m^{-3})
$NPSH$	Net positive suction head (m)
p	Pressure (Pa)
Q	Flow rate (m^3/min)
$\hat{Q}$	Unknown vector
r	Bubble radius (m)
Re	Reynolds number (-)
t	Time (s)
T	Surface tension (N/m)
Δt	Time step (s)
ΔT	Integration time (s)
u, v, w	Velocity (m/s)
U, V, W	Contravariant velocity (m/s)
U_t	Peripheral velocity at impeller blade outlet (m/s)
ΔV	Mesh volume (m^3)
η	Efficiency (-)
κ	Specific heat ratio (-)
μ	Viscosity (Pa s)
Ω	Rotation speed (rad/s)
ρ	Water density (kg/ m^3)
ψ	Head coefficient (-)

Subscripts

cal	Calculation
exp	Experiment
bub, B	Bubble
G	Gas phase
i	x, y, and z directions
j	ξ, η, and ζ directions
L	Liquid phase
R	Three-percent drop in total head
th	Threshold
v	Vapor

REFERENCES

[1] Fukaya, M., et al., 2006, "Experimental Prediction Method of Cavitation Erosion in Pumps by Using Aluminum Sheet," *Proc. 6th Int. Symposium on Cavitation (CAV2006)*, Wageningen, The Netherlands.

[2] Kato, H., 1975, "A Consideration on Scaling Laws of Cavitation Erosion," *Int. Shipbuilding Progress*, Vol.22, No.253, 305-327.

[3] Soyama, H. and Kumano, H., 2002, "The Fundamental Threshold Level – a New Parameter for Predicting Cavitation Erosion Resistance," *Journal of Testing and Evaluation, ASTM International*, 421-431.

[4] Zima, P., Sedlář, M., and Maršík F., 2004, "Bubble Creation in Water with Dissolved Gas: Prediction of Regions Endangered by Cavitation Erosion," *Proc. 14th Int. Conf. on the Properties of Water and Steam (14th ICPWS)*, Kyoto, 232-235.

[5] Fukaya, M, Tamura, Y., and Matsumoto, Y., 2006, "Prediction of Cavitation Intensity and Erosion in Centrifugal Pump Based on Detailed Bubble Behavior Simulated Using Bubble Flow Model," *Proc. 11th Int. Symposium on Transport Phenomena and Dynamics of Rotating Machinery (ISROMAC-11)*, Honolulu, ISROMAC-11_44.

[6] Turbomachinery Society of Japan, 2003, "TSJ Guideline; Guideline for Prediction and Evaluation of Cavitation Erosion in Pumps," *TSJ G 001:2003*. (in Japanese)

[7] Takemura, F. and Matsumoto, Y., 1994, "Internal Phenomena in Bubble Motion," *Bubble Dynamics and Interface Phenomena*, Kluwer Academic Publishers, 467-474.

[8] Knapp, R.T., Daily, J.W., and Hammitt F.G., 1970, "Cavitation : Engineering Societies Monographs," McGraw-Hill Book Company, 76.

[9] Schiller L., and Nauman, A.Z., 1933, "Uber die grundlegenden Berechnungen bei der Schwerkraftaufbereitung," *Ver. Deut. Ing*., Vol. 77, 318-320.

[10] Sridhar, G. and Katz, J., 1995, "Drag and Lift Forces on Microscopic Bubbles Entrained by A Vortex," *Phys. Fluids, 7(2)*, 389-399.

[11] Tamura, Y., Fukaya, M., and Matsumoto, Y., 2002, "Numerical Method for Cavitating Flow Simulations and its Application to Axial Flow Pumps," *Proc. 9th Int. Symposium on Transport Phenomena and Dynamics of Rotating Machinery (ISROMAC-9)*, FD-ABS-129.